

# Distributed fiber-optic temperature sensing for hydrologic systems

John S. Selker,<sup>1,2</sup> Luc Thévenaz,<sup>3</sup> Hendrik Huwald,<sup>2</sup> Alfred Mallet,<sup>2</sup> Wim Luxemburg,<sup>4</sup> Nick van de Giesen,<sup>4</sup> Martin Stejskal,<sup>5</sup> Josef Zeman,<sup>5</sup> Martijn Westhoff,<sup>4</sup> and Marc B. Parlange<sup>2</sup>

Received 7 July 2006; revised 15 September 2006; accepted 27 October 2006; published 6 December 2006.

[1] Instruments for distributed fiber-optic measurement of temperature are now available with temperature resolution of 0.01°C and spatial resolution of 1 m with temporal resolution of fractions of a minute along standard fiber-optic cables used for communication with lengths of up to 30,000 m. We discuss the spectrum of fiber-optic tools that may be employed to make these measurements, illuminating the potential and limitations of these methods in hydrologic science. There are trade-offs between precision in temperature, temporal resolution, and spatial resolution, following the square root of the number of measurements made; thus brief, short measurements are less precise than measurements taken over longer spans in time and space. Five illustrative applications demonstrate configurations where the distributed temperature sensing (DTS) approach could be used: (1) lake bottom temperatures using existing communication cables, (2) temperature profile with depth in a 1400 m deep decommissioned mine shaft, (3) air-snow interface temperature profile above a snow-covered glacier, (4) air-water interfacial temperature in a lake, and (5) temperature distribution along a first-order stream. In examples 3 and 4 it is shown that by winding the fiber around a cylinder, vertical spatial resolution of millimeters can be achieved. These tools may be of exceptional utility in observing a broad range of hydrologic processes, including evaporation, infiltration, limnology, and the local and overall energy budget spanning scales from 0.003 to 30,000 m. This range of scales corresponds well with many of the areas of greatest opportunity for discovery in hydrologic science.

**Citation:** Selker, J. S., L. Thévenaz, H. Huwald, A. Mallet, W. Luxemburg, N. van de Giesen, M. Stejskal, J. Zeman, M. Westhoff, and M. B. Parlange (2006), Distributed fiber-optic temperature sensing for hydrologic systems, *Water Resour. Res.*, 42, W12202, doi:10.1029/2006WR005326.

## 1. Introduction

[2] Hydrologic processes are strongly influenced by interacting processes that span spatial scales from centimeters to kilometers, presenting profound challenges for description, modeling, and observation. Focusing on observation, most in situ sensing systems report data for some sphere of influence centered at a point (e.g., stream gauge, soil moisture, rain gauges). In principle, by placing many such sensors closely spaced along transects it would be possible to observe processes across a range of scales, however this is typically impractical in anything close to an exhaustive manner. In addition, errors between sensors can be large in comparison to actual temperature differ-

ences, for example down a stream. Taking first-order streamflow generation as an example, the contributing area is typically on the order of 1 km<sup>2</sup> (10<sup>6</sup> m<sup>2</sup>). To characterize by point measurements with spheres of influence of 0.1 m<sup>2</sup> (e.g., rain gauge or neutron probe), to cover even 1% of this area would require on the order of hundreds of thousands of sensors, which is in general practically impossible. Though great progress has been made in understanding hydrologic processes within the constraints of point measurements, the ability to physically monitor processes at tens of thousands of points in time could be very revealing of heretofore hidden interactions and processes.

[3] This motivation has brought many new and exciting technologies to hydrologic research in the past decade, largely in the form of remote sensing [e.g., *Schultz*, 1988; *Schmugge et al.*, 2002]. Several tools have allowed for sub-1-m<sup>2</sup> resolution: airborne laser scanning [e.g., *Wehr and Lohr*, 1999] has allowed characterization of landscape surface elevation and vegetation density; satellite imagery has allowed documentation of spectral response and temperature; and lidar [e.g., *Pinzón et al.*, 1995] has facilitated observation of the distribution of humidity in space and time; forward looking infrared (FLIR) has provided temperature at sub-1-m resolution that can be used to characterize a variety of hydrologic parameters [*Loheide and Gorelick*, 2006]. Each of these now well known technolo-

<sup>1</sup>Department of Biological and Ecological Engineering, Oregon State University, Corvallis, Oregon, USA.

<sup>2</sup>School of Architecture, Civil and Environmental Engineering, Ecole Polytechnique Fédérale de Lausanne, Lausanne, Switzerland.

<sup>3</sup>Laboratoire de Nanophotonique et Métrologie, Ecole Polytechnique Fédérale de Lausanne, Lausanne, Switzerland.

<sup>4</sup>Water Resources, Faculty of Civil Engineering and Geosciences, Delft University of Technology, Delft, Netherlands.

<sup>5</sup>Institute of Geological Sciences, Faculty of Science, Masaryk University, Brno, Czech Republic.

gies has fundamentally transformed our ability to understand hydrological processes, and allowed us to test conceptual models that synthesize our understanding across scales.

[4] In this communication we introduce a family of fiber-optic technologies that may be of use in the direct sensing of hydrologic processes by expanding the scales over which measurements of temperature can be made.

## 2. Principles, Pros, and Pitfalls

[5] The general concept behind the use of fiber optics for distributed sensing is to observe the conditions found at a particular distance along the fiber from the instrument by virtue of the time of travel of light in the fiber. This technique has been employed in groundwater applications to a limited degree (e.g., borehole monitoring [Henninges *et al.*, 2003] and aquifer characterization [MacFarlane *et al.*, 2002]) and to a much greater degree in civil infrastructure [e.g., Measures, 2001]. The spatial resolution of such time domain measurements is limited by the ability to resolve a signal in time (instrument performance), and the dispersion of signals within the fiber (sensor performance). The precision of such measurements are affected by factors such as signal-to-noise ratio, measurement drift, and cross sensitivities. By briefly considering the underlying physics of each system, the expectations for precision and utility are revealed in their broadest sense.

### 2.1. Mechanical Change in Size: Fiber Bragg Grating

[6] Before addressing truly distributed techniques, we mention a semidistributed fiber-optic method that may be valuable in selected applications. In contrast to the following methods, this method does not rely on time of travel, but rather monitors the net adsorption of particular frequencies of light within the fiber. A fiber Bragg grating (often abbreviated as FBG) is a very short (of the order of microns) section of optical fiber on which the outer refractive index barrier has been etched with an optical grating (i.e., a very closely spaced set of “scratches” on the surface of the fiber) that will filter a very tightly constrained frequency of light, with wavelength specificity of on the order of one nanometer (for a general introduction to the subject, see Kashyap [1999], Othonos [1997], or other introductory texts). The “reading” of each grating consists of measuring the precise frequency of the adsorption band of the grating. If a spectrum of light is transmitted along this fiber, each grating will adsorb light at a very specific range of wavelengths proportional to the spacing of the etching. Since the frequency response of the gratings is a function of the spacing of the lines of the grating, any process that changes this spacing can be monitored. Most prominently, the line spacing may change when the fiber expands and contracts with changes in temperature and mechanical stress on the fiber. As many as 100 such gratings may be distributed along a fiber, with the adsorption peak of each grating identified using a frequency-scanning laser. Each grating acts as a point of measurement. The gratings may be spaced as closely as 0.1 mm, or as widely as allowed by cable attenuation (on the order of 10 km). Using time domain information it is possible to isolate a series of gratings along a fiber, thus extending the possible number of gratings that

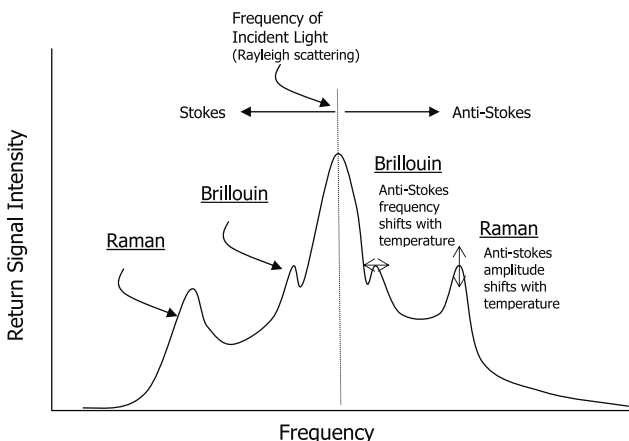


**Figure 1.** Diagram of Rayleigh, Raman, and Brillouin return scattering intensity below (Stokes) and above (anti-Stokes) the frequency of the injected light.

can be read, but also increasing the complexity of the measurement instrument.

[7] With the gratings each tuned to different frequencies, the measurement can be made without respect to time of travel, with each adsorption peak corresponding to a specified grating. As the ability of engineers to control the etched spacing improves, so does the ability to resolve temperature and stress. Current technology allows for measurement of changes in temperature with precision approaching  $0.1^{\circ}\text{C}$  [Rao *et al.*, 1997]. The gratings themselves can be made at micron scales, so that distinct measurements may be obtained at spatial resolutions equal to the cable diameter ( $<100\ \mu\text{m}$ ), sufficient for the hydrologic applications of which we are aware. A key distinction between Bragg gratings and the techniques discussed hereafter is the requirement that the fiber be modified at the point of measurement (e.g., the etched grating). The etching process is technically demanding, and so this technique is currently rather expensive per point of measurement.

### 2.2. Mechanical Change in Density: Brillouin Scattering

[8] Even in the purest optical fibers, light is scattered as a result of the disordered (noncrystalline) structure of glass. Three primary modes of scattering are Rayleigh (elastic), Brillouin, and Raman (both nonelastic). The elastic scattering gives rise to a backscattered signal with no wavelength change, while the two nonelastic scattering phenomena result in light at wavelengths greater than (Stokes) and less than (anti-Stokes) the primary laser light (Figure 1). In the case of Brillouin scattering, the effect is the result of subtle density shifts in the fiber caused by electromagnetic forces from the passage of intense laser light [e.g., Kurashima *et al.*, 1990; Niklès *et al.*, 1997]. These density changes propagate as acoustic waves, or phonons, giving rise to an intense resonant phenomenon. The wavelength shift of the Stokes and anti-Stokes scattered light is then proportional to the acoustic velocity of the fiber, which is a function of the fiber density. This velocity is highly correlated to the  $\text{GeO}_2$  content of the fiber, which varies by manufacturer and is not included in fiber specifications, thus each producer's fiber must be calibrated. As seen for the Bragg gratings, the

density thus measured can be used to determine changes in temperature or stress. Standard fiber-optic communication cables hold the fiber in a stress-free condition, ideally suited to the temperature measurement application, as shown in Figure 2 where the lake bed temperature is shown for three dates using Brillouin scattering. Though beyond the scope of this article, there are two very different strategies to measure Brillouin scattering, referred to as spontaneous and stimulated. While quite different with respect to the tools of measurement, the overriding principles and limitations are similar.

[9] The key to making a Brillouin scattering measurement is the identification of the shift in wavelength of the scattered light. Because the scattered light wavelengths fall into a Gaussian distribution, the precision of determination of the center of the shift is a statistical computation limited by the standard deviation of this distribution to about  $\pm 0.1^\circ\text{C}$  [Niklès *et al.*, 1997]. Since the measurement relies on taking averages of many independent backscatter events, the precision of the reading is a function of the time allowed for sampling. Thus the precision will be less for rapidly changing temperatures, with the reported value reflecting the average temperature over the sampling interval. The time domain-based spatial resolution of these measurements is limited by the length of the optical pulse required to activate the scattering through electromagnetic forces, yielding a best resolution of 0.5 to 1.0 m as a result of the narrow band process limiting the optical signal to a bandwidth of about 100 MHz. Brillouin scattering can be made on standard single-mode fiber-optical cables as employed in telecommunications, as was the case in the study shown in Figure 2 under Lake Geneva. Commercial Brillouin-based distributed temperature sensor (DTS) systems have the capability to measure along cables of lengths to 30,000 m, with possibilities of extension up to 150,000 m (e.g., Omnisens, Lausanne, Switzerland).

### 2.3. Optical Change in Scattering: Raman

[10] When light strikes matter the light may be reflected at the original energy, or a portion of that light is adsorbed and reemitted at wavelengths just above and below the frequency of the incident light due to loss or gain from quanta of energy exchanged with electrons. This frequency-shifted light is referred to as Raman scattering, with the light at frequency below the incident light being referred to as Stokes backscatter, and that above the incident light the anti-Stokes backscatter (Figure 1). Below a critical light intensity the magnitude of Raman Stokes scattering is a linear function of the intensity of illumination, while at these intensities the anti-Stokes scattering is a function of the intensity of illumination and exponentially of the temperature of the fiber. Hence the ratio of the magnitudes of the anti-Stokes to Stokes scattered light eliminates the intensity dependence and provides a quantity that depends exponentially on the fiber temperature (Figure 1). The precision of this measurement is limited primarily by the accuracy of this ratio, a function of the total number of photons observed, specifically to the standard deviation of this computed ratio, which will be by the law of large numbers follow a normal distribution decreasing with the square root of the total number of photons observed. Hence the precision of temperature measurements will increase with the square root of the integration interval, as long as instrument

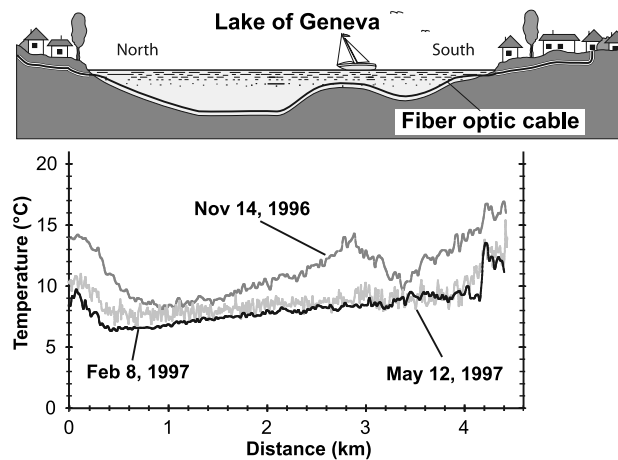


**Figure 2.** Temperature transects taken between France (south) and Switzerland (north) using existing communication fibers under Lake Geneva obtained using stimulated Brillouin scattering.

drift and other sources of error are insignificant. At the same time, the greater the spatial resolution, the fewer photons observed per unit time per interval of measurement, resulting in a lower rate of temperature reading convergence. The strength of the optical signal decays exponentially with distance from the source (Beers law), so points further from the instrument have lower photon counts, and will therefore also require proportionally longer integration times to obtain a desired level of precision. In summary, the precision of a Raman measurement is, to first approximation, proportional to the square root of the product of the linear distance from the instrument and the number of resolved sections divided by the integration time. As a rule of thumb, based on current technology (depending on the intensity of the lasers and other factors), a measurement with 1 m spatial resolution taken 1000 m from the instrument and integrated for 1 min will have a standard deviation of on the order of  $0.1^\circ\text{C}$ , depending strongly on laser intensity and detector sensitivity. Measurements averaged over an hour can reach the  $0.02^\circ\text{C}$  level, and after 24 hours this precision could be achieved along an entire 10,000 m cable.

[11] One might think that this could be improved to an arbitrary degree by using more intense lasers, but this approach is limited by the optical nonlinearity in the scattering that arises at high intensities: it is critical to keep the intensity below this threshold. To obtain the greatest photon count suggests the use of a larger diameter ( $50\ \mu\text{m}$  diameter, or roughly  $2000\ \mu\text{m}^2$ ) multimode fiber, which is no longer employed in long-haul communications due to the higher dispersion. On the contrary, standard  $9\ \mu\text{m}$  diameter single-mode cable has almost negligible dispersion, but the allowable signal strength is reduced by a factor of 25 due to the smaller cross section. Because of the greater optical dispersion, the spatial resolution of Raman scattering systems is limited to on the order of 1 m for lengths up to 1000 m, and up to 2 m for lengths up to 10,000 m. Spatial resolution to as little as 30 cm can be achieved for shorter cables ( $<1000$ ), but this requires much more expensive lasers, longer integration times, and low-dispersion fibers.



[12] There are several instrument manufacturers providing Raman-based DTS equipment, with instruments having significantly differing specifications. Most of the systems are designed for indoor instrument placement and standard AC power applications that can be logistically challenging in field hydrology. The DTS options are quickly expanding as the market sees the need for environmental sensing systems that may be off the grid and without the protection of a building. As an example, Agilent's N4386A that came to market in May of 2006 is designed for remote applications, operating on less than 40 W at 12 V (well suited to solar panel power supply), and with allowable operating conditions spanning  $-10^{\circ}$  to  $60^{\circ}\text{C}$ . Systems have varying sensitivity to ambient temperature which is an area of concern in outdoor applications, and should be explored with manufacturers per application. An important aspect to keep in mind is that this is a technology that provides temperature data with minimal setup or interpretation required. It is necessary to calibrate the instrument to the cable by attaching the fiber-optic cable to the instrument with the cable in an environment of well-known temperature. The calibration typically requires a value of temperature offset, and a slope parameter that adjusts the offset with distance from the instrument. The calibration is carried out by placing the cable in an environment of known constant temperature, attaching the cable to the DTS, and taking a long-time integration data set. Thus the absolute precision of device is typically limited by the accuracy of the calibration, while the precision of observing changes in temperature is a function of the DTS, and is typically on the order of  $0.01^{\circ}\text{C}$ . Once calibrated, the instrument directly reports temperature for each meter (or other user-specified interval) of cable.

### 3. Examples of Hydrologic and Water Resource Applications

[13] There are many applications of temperature measurements in the observation of hydrological processes, for instance in computing the energy balance for evaporative loss, the condition of aquatic environments, or as a tracer of convection. In most cases it is useful to measure gradients in temperature in time and space. In the case of hillslope hydrology, one might consider an installation of a series of parallel fiber-optic cables vertically in a soil profile to be able to obtain the energy balance of the soil for the determination of evaporation, as well as allowing the observation of advected temperature profiles due to infiltration. Fiber-optic cables can be multiplexed to allow reading of temperatures along numerous fibers with a single instrument. In this paper we present five illustrative applications that are not comprehensive, but demonstrate the range of configurations and environments where the DTS approach could be used. They are (1) the measurement of lake bottom temperatures along communication cables (2) the measurement of the temperature profile with depth in a 1,400 m deep decommissioned mine shaft, (3) the measurement of the air-snow interface temperature profile above a snow covered glacier, (4) the measurement of air-water interfacial temperature in a lake, and (5) the temperature distribution along a first-order stream. The first example employs Brillouin scattering, while the remaining applications made use of Raman scattering-based instrumentation. These

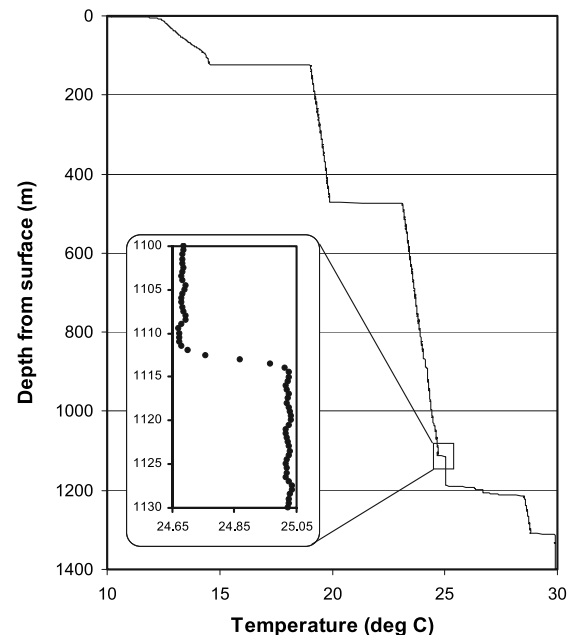


**Figure 3.** Vertical temperature profile of the Jindrich Coal mine in the Czech Republic, 5 April 2006, based on 24 hour averaged data. The inset expands the data about the smallest temperature step between strata. Data points are separated by 0.5 m as reported by the instrument.

examples are presented to illustrate the potentially transformative nature of the data that could be obtained using such a system. Except for the first, these examples draw upon data collected in April and May of 2006. The presentation given here is very brief for the purpose of demonstrating the potential of the DTS system rather than being scientifically comprehensive. These data will be more fully explored for their scientific implications in later publications.

#### 3.1. Example 1: Temperature at the Bed of Lake Geneva Measured With Stimulated Brillouin Scattering

[14] Because the DTS method does not require specialized fiber-optic cables, the measurements may be made opportunistically using telecommunications infrastructure. In this example the measurement of seasonal temperature profiles along the bed of Lake Geneva were conducted using Brillouin scattering along a spare telecommunications cable (Figure 2). As well as directly providing information of aquatic conditions along the lakebed, such data could be valuable for the validation of lake circulation and energy balance models. These data were taken using a laboratory-constructed “first-generation” instrument at a wavelength of 1319 nm achieving spatial resolution of 3 m with 20 min integration time and a maximum range of 10 km with precision of approximately  $0.25^{\circ}\text{C}$ . This compares with the current performance of commercially produced Brillouin instruments that operate at 1550 nm wavelength that have a range 30 km, spatial resolution of 1m, and measurement time 1 min for  $0.1^{\circ}\text{C}$  precision (e.g., the Brillouin DTS Omnisens DiTeST, Lausanne, Switzerland).

#### 3.2. Example 2: Temperature Profile of a Decommissioned Mine Shaft

[15] In the Czech Republic there are many decommissioned mines. Some of these mines have now been flooded

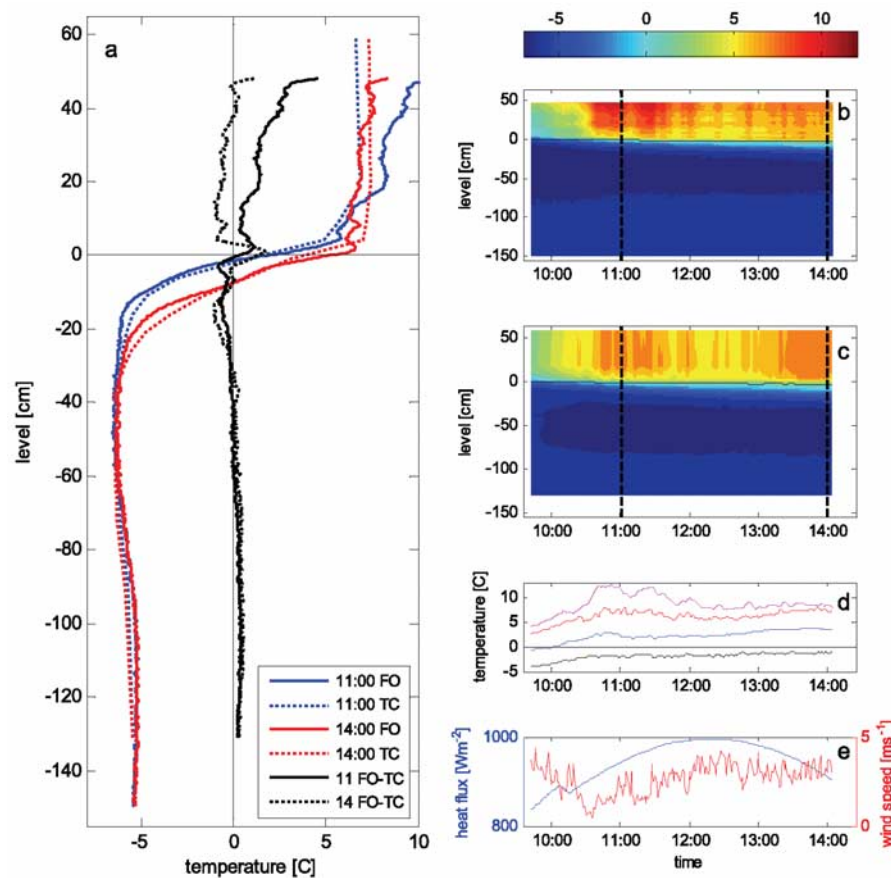


**Figure 4.** Comparison of fiber-optic (FO) and thermocouple (TC) temperature profilers on the Glacier de la Plaine Morte, Switzerland, 14 April 2006. (a) Temperature profiles taken in the morning and afternoon (compare dashed lines in Figures 4b and 4c; zero elevation is the location of the air-snow interface). Time evolution of temperature for (b) FO and (c) TC (employing the same color-scale for temperature shown in Figure 4a). (d) Air temperature as measured by the fiber-optic and thermocouple systems (data taken at 50 cm, pink and red lines), a shielded passively ventilated sensor (Rotronic 103A T/RH, blue line), and infrared temperature from upward longwave radiation (electrically ventilated Kipp & Zonen CG4, solid black line). (e) Incoming shortwave heat flux (blue line) and wind speed (red line). The small S curve in the heat flux was due to backscatter caused by ice accumulation on the sensor that melted off at 10:10 AM.

and, further, have mine waters entering surface waters. The composition of these mine shaft drainage waters is of considerable environmental interest. In recent years it has been noted that the surface outflows of mine effluent can suddenly increase in contaminant concentration following many years of relatively constant quality [e.g., Kalous *et al.*, 2005]. Investigation demonstrated that the mineshafts were stratified, with more contaminated warmer water at the bottom of shafts held in place by greater density due to dissolved solids below cooler but less contaminated waters. To study the structure and temporal properties of the stratified system we employed a Raman system (Sensornet Sentinel DTS-LR, London, England), using Brusens (Brugg Cables, Switzerland) fiber-optic cable (Figure 3). The thermal strata within the mine are readily identified: the air-water interface occurs at 122.5 m, with separation of temperature strata at 472, 1123, a series between 1190 and 1213, and 1310 m. Although there are lateral excavations off the upper 1,200 m of the shaft, the lowest 100 m is a simple vertical shaft. The shaft may be seen to have

stratified from warm at the bottom to cool at the top with the layers stabilized by the high dissolved solids concentrations. Over a 24 hour period the temperature was constant vertically with standard deviation of  $0.007^{\circ}\text{C}$ , supporting the manufacturer's contention that the system is able to distinguish  $0.01^{\circ}\text{C}$  changes in temperature.

[16] The spatial resolution of the system is revealed in the reported temperatures across the strata divisions. Independent wireline measurements of temperature showed that the strata transition occurs in less than 0.10 m. Therefore these transitions may be taken to be a perfect step function from the perspective of the DTS. The DTS instrument was setup to report the temperature every 0.5 m, understanding that due to dispersion and laser pulse length the true resolution would be greater than this. The step highlighted in Figure 3 illustrates that the system completes over 90% of the temperature transition within 1 m a distance 1100 m from the instrument, supporting the manufacture's claim of 1 m spatial resolution.

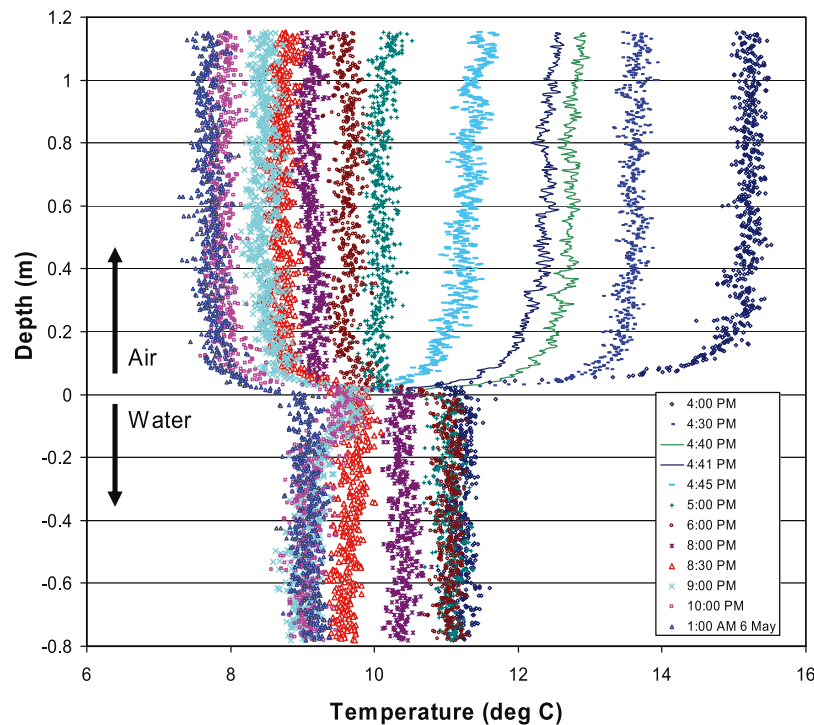


**Figure 5.** Temperature profiles obtained in Lake Geneva 20 m from shore at St. Sulpice, Switzerland, 5 May 2006, as a minor thunderstorm overtook the site. All data points were obtained using 15 s integrations, while the solid lines represent 1-min integrations illustrating the relationship between integration time and scatter.

### 3.3. Example 3: Air-Snow Interface Temperature Profile Above a Glacier

[17] There is great interest in the energy balance of snow systems to better understand the vulnerability of snow to global climate change. Fundamental to understanding the dynamics of energy transfer within snow is measurement of the dynamics of the temperature within a snowpack. We desired a measurement system that would provide resolution of 5 mm in the vertical with  $0.05^{\circ}\text{C}$  in temperature, and 5 min in time. By helically wrapping 500 m of plastic encased multimode cable (outer diameter =  $900\text{ }\mu\text{m}$ ) about a 0.075 m diameter PVC pipe, the entire 500 m fiber was compressed onto a 2 m measurement section. Each meter of fiber corresponded to 4 mm vertically along the probe. The entire probe was wrapped in two layers of aluminized Mylar to limit radiant energy adsorption. With 2 min integration time the DTS (Sentinel DTS-LR, SensorNet London, England) achieved  $0.05^{\circ}\text{C}$  standard deviation in temperature. Thus the basic resolution requirements were met. The DTS-based system was located 1 m from a thermocouple-based system consisting of a 0.05 m diameter tube with thermocouples placed at 25 mm intervals near the air-snow interface and larger intervals of 10 cm above and 50 cm below the interface. The two systems agreed well at common depths, though the DTS provided both greater vertical and temperature resolution (Figure 4). The two methods agreed to within less than  $1^{\circ}\text{C}$  below the snow surface, while above the snow the aluminized Mylar wrapped fiber-optic system was more susceptible to solar heating (up to  $12^{\circ}$  above ambient) than was the painted white thermocouple system (up to  $7^{\circ}$  above ambient:

Figure 4d). From 0.2 m above the interface to the full depth of the sensors the systems agreed within  $1^{\circ}$  (Figure 4a).

### 3.4. Example 4: The Measurement of Air-Water Interfacial Temperature in an Alpine Lake

[18] The probe employed in example 3 was also installed in a 0.85 m deep location in Lake Geneva, 20 m from the shore and read with a DTS (Sentinel DTS-LR, SensorNet, London, England) read at 15 s intervals (Figure 5). It can be seen that the air temperature dropped precipitously between 4:40 and 4:41 PM (approximately  $0.4^{\circ}/\text{min}$ ) when a thunder storm passed the site. The water temperatures also fell rapidly, though almost 4 hours later. Note that between 8:00 and 8:30 the water column cooled by  $0.8^{\circ}\text{C}$ , presumably through mixing with cooler deep water driven by the storm winds. The logarithmic temperature profile in the air in the first 30 cm above the lake provides data useful to the computation of the sensible heat flux.

### 3.5. Example 5: The Temperature Distribution Along a First-Order Stream

[19] In streams and rivers water temperature is of importance to ecological processes, and may also be useful to determine inputs of both surface and groundwaters to streams. In this case a fiber (Brusense, Brugg, Switzerland) was installed in the Maisbich, a groundwater-fed first-order stream in Luxembourg and read with the DTS (Sentinel DTS-LR, SensorNet, London, England) (Figure 6). The data shown were taken on a sunny day that transitioned to a clear sky night. Groundwater inputs and confluences are apparent, giving temperature measurements of unprecedented precision and resolution both temporally and spatially.



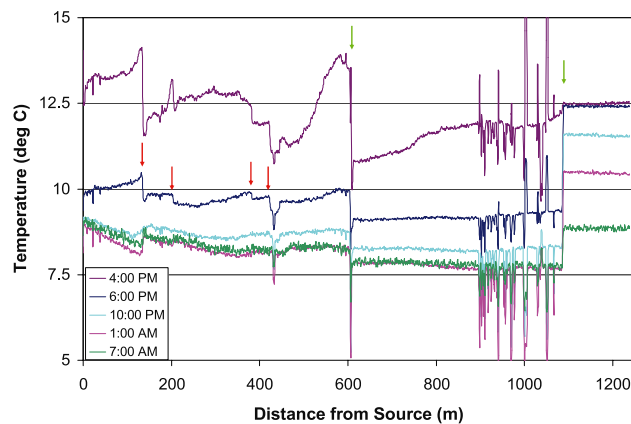


**Figure 6.** Temperature profiles from the source (0 m) through two confluences (green arrows, joining a stream of approximately equal size at 608 m and a stream approximately an order of magnitude larger at 1087 m) along Luxembourg's Maisbich taken 24–25 April 2006. All data are 12 min averages except 7:00 AM, which is a 2 min average. Red arrows show points of groundwater input. At 430 m the stream cascades down a small waterfall, and between 896 m and 1065 m the stream flows over stepped bedrock, leaving the cable frequently exposed to air in both cases.

These data open many opportunities for quantifying stream processes. For instance, by choosing specific times at which stream temperature does not change at the point of a known groundwater input (see the 10:00 PM trace of Figure 6 at position 150 m for example) it is possible to identify the local groundwater inflow temperature. Using gauges of surface water flux along the flow path, the changes in temperature at points of groundwater input allows for accurate estimates of point-wise groundwater inputs based on an energy balance.

#### 4. Apparent Precision of Measurements

[20] In this work we have sought to demonstrate the application of a temperature measurement methods that has long since been calibrated and validated with respect to limitations imposed by instrumentation. Among the data shown, however, several indications of the precision of the method can be deduced. Figure 5 (Lake Geneva temperature profiles) shows data taken on 15 and 60 s intervals to illustrate the precision of short-interval data sets, while Figure 3 (mine shaft) illustrates long-interval integration (1 day). The 15 s data of the air-lake interface have a standard deviation of  $0.14^{\circ}\text{C}$ , the 1 min data has a standard deviation of  $0.06^{\circ}\text{C}$ , while a  $0.007^{\circ}\text{C}$  standard deviation is obtained during full-day integration, believed to be limited not by the instrument, but by actual fluctuations in temperature.

#### 5. Conclusions

[21] Although distributed temperature measurement using fiber-optic sensing has been possible for over a decade, only in very recent years have accurate, robust, affordable, and user-friendly systems been developed. The field of available

instruments is rapidly expanding while costs have decreased, and all indications suggest that this trend will continue. There are a number of quite distinct methods that have been developed, each with features that must be understood if a successful experiment is to be carried out. Installation of the cables often presents significant logistical challenges, but the mature fiber-optic communications field has developed many specialized tools for this as well. We believe that the potential to span more than six orders of magnitude in spatial scale demonstrated here opens a wide variety of tremendous opportunities for application of this technology in hydrology where scaling behavior across the 0.01–10,000 m range is a central challenge to current understanding in surface water, near-surface, and atmospheric processes.

[22] **Acknowledgments.** We thank Martin Tromp for his technical assistance, which made possible several of the field trials. We thank the EPFL, the Swiss National Science Foundation (grants 109566 and 107910), the Oregon Experiment Station, the U.S. National Science Foundation (grant 0447415-EAR), and Masaryk University for their financial support of this work. The work in Luxembourg was supported by Water Research Centre Delft and the Municipality of Ettelbruck. We gratefully acknowledge the insights and suggestions of Michael Gooseff and the anonymous reviewer. These comments significantly enhanced the presentation of this work.

#### References

- Henningses, J., G. Zimmermann, G. Büttner, J. Schrötter, K. Erbas, and E. Huenges (2003), Fibre-optic temperature measurements in boreholes, paper presented at the 7th FKPE-workshop "Bohrlochgeophysik und Gesteinsphysik," GeoZentrum Hannover, Hannover, Germany, 23–24 Oct.
- Kalous, J., A. Kopriva, J. Havelka, and J. Zeman (2005), Seasonal and long-term mine water evolution in Czech Republic, paper presented at 20th World Mining Congress and Expo 2005, Minist. of Ind. and Mines, Tehran, 7–11 Nov.
- Kashyap, R. (1999), *Fiber Bragg Gratings*, 458 pp., Elsevier, New York.
- Kurashima, T., T. Horiguchi, and M. Tateda (1990), Distributed-temperature sensing using stimulated Brillouin scattering in optical silica fibers, *Opt. Lett.*, 15(18), 1038–1040.
- Loheide, S. P., and S. Gorelick (2006), Quantifying stream-aquifer interactions through the analysis of remotely sensed thermographic profiles and in situ temperature histories, *Environ. Sci. Technol.*, 40, 3336–3341.
- MacFarlane, A. P., A. Förster, D. Merriam, J. Schrötter, and J. M. Healey (2002), Monitoring artificially stimulated fluid movement in the Cretaceous Dakota aquifer, western Kansas, *Hydrogeol. J.*, 10(6), 662–673.
- Measures, R. M. (2001), *Structural Monitoring With Fiber Optic Technology*, 716 pp., Elsevier, New York.
- Niklès, M., L. Thévenaz, and P. A. Robert (1997), Brillouin gain spectrum characterization in single-mode optical fibers, *J. Lightwave Technol.*, 15(10), 1842–1851.
- Othonos, A. (1997), Fiber Bragg gratings, *Rev. Sci. Instrum.*, 68(12), 4309–4341.
- Pinzón, J. E., C. E. Puente, M. B. Parlange, and W. Eichinger (1995), A multifractal analysis of lidar measured water vapour, *Boundary Layer Meteorol.*, 76(4), 323–347.
- Rao, Y.-J., D. J. Webb, D. A. Jackson, L. Zhang, and I. Bennion (1997), In-fiber Bragg-grating temperature sensor system for medical applications, *J. Lightwave Technol.*, 15(5), 779–785.
- Schnugge, T. J., W. P. Kustas, J. C. Ritchy, T. J. Jackson, and A. Rango (2002), Remote sensing in hydrology, *Adv. Water Resour.*, 25(8), 1367–1385.
- Schultz, G. A. (1988), Remote sensing in hydrology, *J. Hydrol.*, 100, 239–265.
- Wehr, A., and U. Lohr (1999), Airborne laser scanning—An introduction and overview, *J. Photogramm. Remote Sens.*, 54, 68–82.

H. Huwald, A. Mallet, and M. B. Parlange, School of Architecture, Civil and Environmental Engineering, Ecole Polytechnique Fédérale de Lausanne, CH-1015 Lausanne, Switzerland.

W. Luxemburg, N. van de Giesen, and M. Westhoff, Water Resources, Faculty of Civil Engineering and Geosciences, Delft University of Technology, Stevinweg 1, NL-2628 CN Delft, Netherlands.

J. S. Selker, Department of Biological and Ecological Engineering, 116 Gilmore Hall, Oregon State University, Corvallis, OR 97331, USA. (selkerj@engr.orst.edu)

M. Stejskal and J. Zeman, Institute of Geological Sciences, Faculty of Science, Masaryk University, Žerotínovo nám. 9, 601 77 Brno, Czech Republic.

L. Thévenaz, Laboratoire de Nanophotonique et Métrologie, Ecole Polytechnique Fédérale de Lausanne, CH-1015 Lausanne, Switzerland.